Nano Research
2023, 16(4): 5357–5367

ISSN 1998-0124 CN 11-5974/O4
https://doi.org/10.1007/s12274-022-5254-x

Research Article

A lipid-based LMP2-mRNA vaccine to treat nasopharyngeal carcinoma

Mengran Guo[1,§], Xing Duan[1,§], Xingchen Peng[1,2,§], Zhaohui Jin[1,2], Hai Huang[1], Wen Xiao[1], Qian Zheng[1], Yongqi Deng[1], Na Fan[1], Kepan Chen[1], and Xiangrong Song[1] (✉)

[1] *Department of Critical Care Medicine, Department of Clinical Pharmacy, Frontiers Science Center for Disease-related Molecular Network, State Key Laboratory of Biotherapy and Cancer Center, West China Hospital, Sichuan University, Chengdu 610000, China*
[2] *West China School of Pharmacy, Sichuan University, Chengdu 610000, China*
[§] *Mengran Guo, Xing Duan, and Xingchen Peng contributed equally to this work.*

Received: 26 August 2022 / **Revised:** 22 October 2022 / **Accepted:** 27 October 2022

ABSTRACT

Nasopharyngeal carcinoma (NPC) is a serious and highly invasive epithelial malignancy that is closely associated with Epstein–Barr virus (EBV). Due to the lack of therapeutic vaccines for NPC, we selected EBV latent membrane protein 2 (LMP2) as a preferable targeting antigen to develop a lipid-based LMP2-mRNA (mLMP2) vaccine. Full-length mLMP2 expressing LMP2 was first synthesized using an *in vitro* transcription method and then encapsulated into (2,3-dioleacyl propyl) trimethylammonium chloride (DOTAP)-based cationic liposomes to obtain the mRNA vaccine (LPX-mLMP2). The cell assays showed that the antigen-presenting cells were capable of highly efficient uptake of LPX-mLMP2 and expression of LMP2. LMP2 could subsequently be presented to form the peptide-major histocompatibility complex (pMHC). Furthermore, LPX-mLMP2 could accumulate in the spleen, express antigens, promote the maturation of dendritic cells and stimulate antigen-specific T-cell responses *in vivo*. It dramatically inhibited the tumor growth of the LMP2-expressing tumor model after three doses of vaccination. Additionally, the proliferation of antigen-specific T cells in the tumor site made a good sign for the promise of mRNA vaccines in virus-induced cancer. Overall, we provided a newly developed antigen-encoding mRNA vaccine with advantages against NPC. We also demonstrated that mRNA vaccines are attractive candidates for cancer immunotherapy.

KEYWORDS

mRNA vaccine, latent membrane protein 2 (LMP2), nasopharyngeal carcinoma, Epstein–Barr virus (EBV), tumor-infiltrating lymphocytes

1 Introduction

Nasopharyngeal carcinoma (NPC) is the most common malignant cancer of the head and neck and is mainly prevalent in East and Southeast Asia. According to statistics, there were 133,354 new cases and 80,008 new deaths worldwide in 2020 [1]. The primary treatment regimens for NPC are radiation and chemotherapy. They could offer good prognosis for NPC at early-stage and intermediate stages, while local recurrence and distant metastasis always result in treatment failure and low survival rates [2, 3].

Epstein–Barr virus (EBV) is a common pathogen, and more than 90% of adults globally are estimated to be infected with EBV [4]. EBV infection is closely associated with NPC and contributes the most cases. Latent EBV antigens with good immunogenicity are capable of activating antigen-specific cytotoxic T lymphocytes (CTLs), which have become the focus of immunotherapies against EBV-associated malignancies [5]. Thus, therapeutic EBV vaccine strategies are promising in the treatment of NPC [6]. Some of the strategies have been in clinical trials, including dendritic cell (DC)-based vaccines [7] and recombinant viral vector-based vaccines [8, 9]. DC-based EBV vaccines have shown effectiveness and safety in responders. However, the broad application of DC-based EBV vaccines may not be feasible due to the cost associated with the preparation of personalized vaccines. Recombinant viral vector-based vaccines, such as the modified vaccinia ankara (MVA) vector vaccine and adenoviral vector vaccine, have been shown to boost EBV-specific $CD8^+$ and $CD4^+$ T-cell responses in NPC patients. However, safety, such as the integration risk of viral genes into the host genome, needs to be further evaluated. Thus, it is necessary to develop novel vaccines with higher immunogenicity and safety.

mRNA therapy has attracted much more attention and has become a novel appealing approach in fighting large-scale outbreaks of infectious diseases [10]. For example, the wide application of mRNA vaccines in the prevention of SARS-CoV-2 displayed high immunogenicity and good tolerance in healthy people [11]. It is also widely applied in cancer [12, 13], gene diseases [14], and reactivation of the tumor suppressor [15]. mRNA vaccines can transfect antigen presenting cells (APCs), such as DCs, where the antigen-encoding mRNA is capable of being translated into functional antigen proteins. The proteins are presented via major histocompatibility complex (MHC) molecules and then activate the CTLs to further kill the tumor cells. mRNA

Address correspondence to xiangrong_11@126.com

can be transiently translated in cells, degraded in a short time [16, 17], and not supposed to enter the nucleus. These features allow more controlled antigen exposure, making it safer and more efficient. In the recent a few decades, mRNA vaccines have shown promise in several types of cancers, including pancreatic cancer [18], melanoma [19], glioblastoma [20], and prostate cancer [21]. However, the effectiveness of mRNA vaccines in treating virus-induced cancers remains unknown.

Cancer cells can express a series of inhibitory cytokines, enzymes, and checkpoint molecules and recruit immunosuppressive immune cells, making the tumor microenvironment (TME) a highly immunosuppressive state [22, 23]. In NPC patients, EBV-related tumor cells mainly express EBV nuclear antigen 1 (EBNA1) and latent membrane protein 1 (LMP1) and LMP2 antigens. These antigens are critical for the release of various cytokines to recruit and promote the homing of lymphocytes and other immune cells to the TME. However, in the early stage, EBNA1-specific $CD8^+$ T-cell responses are suppressed by reducing the recognition of T cells [24]. LMP1 can promote cell motility, invasion, and metastasis [25] and is unsuitable as a therapeutic target. LMP2 is expressed more consistently in NPC patients. It can prevent the activation of lytic EBV replication and maintain EBV latency by blocking tyrosine phosphorylation [26]. In addition, LMP2 contains many $CD8^+$ T-cell epitopes [27, 28] and is therefore considered the best $CD8^+$ T-cell target expressed in NPC. It was reported that using multiepitope EBV-LMP2 as an antigen would increase EBV-specific $CD8^+$ and $CD4^+$ T-cell responses in NPC patients [7–9, 29–31]. Thus, in this study, LMP2-mRNA (mLMP2) expressing full-length LMP2 was synthesized using an *in vitro* transcription method. Cationic liposomes were used to encapsulate mLMP2 (LPX-mLMP2) to enhance the stability and delivery of mRNA. Then, the *in vitro* characterization, antigen expression and presentation, pharmacodynamics against NPC, and the mechanism were investigated. It was shown that LPX-mLMP2 was a promising mRNA vaccine against NPC.

2 Materials and methods

2.1 Materials and reagents

(2,3-Dioleacyl propyl) trimethylammonium chloride (DOTAP), 1,2-di-O-octadecenyl-3-trimethylammonium propane (chloride salt) (DOTAM), and 3ß-[N-(N', N'-dimethylaminoethane)-carbamoyl] cholesterol hydrochloride (DC-Chol) were purchased from A.V.T. Pharmaceutical Co., Ltd. (Alabaster, USA). G0-C14 was synthesized and purified by published protocols [15, 32]. Cholesterol (Chol) was supplied by Shanghai Yuanju Biology Technology Company (Shanghai, China). mLMP2, mRNA encoding ovalbumin (mOVA), and mRNA encoding green fluorescent protein (mGFP) were synthesized in the State Key Laboratory of Biotherapy at Sichuan University. Cy5-conjugated mRNA (mCy5) and mRNA encoding luciferase (mLUC) were purchased from TriLink Biotechnologies (San Diego, CA, USA). D-Luciferin (potassium salt) was purchased from Biovision. 1× tris-acetate-ethylenediaminetetraacetic acid (TAE) buffer, agarose, 1,1'-dioctadecyl-3,3,3',3'-tetramethylindodicar-bocyanine, 4-chlorobenzenesulfonate salt (DiD), RNase-free water, and erythrocyte lytic products were obtained from Sigma –Aldrich (Shanghai), Inc. (Shanghai, China). Granulocyte-macrophage colony-stimulating factor (GM-CSF) was purchased from Pepro Tech Inc. (Rocky Hill, USA). APC-anti-mouse CD11c, PE-anti-mouse CD11c, phycoerythrin (PE)-anti-mouse CD80, fluorescein isothiocyanate (FITC)-anti-mouse CD86, and APC-anti-mouse SIINFEKL/H-2Kb 25-D1.16 were purchased from Biolegend Inc. (San Diego, CA, USA). FITC-anti-mouse CD3, APC-anti-mouse CD8a, and PE-anti-mouse CD4 were obtained from Becton Dickinson and Company (New York, USA); PE-H-2Kb SIINFEKL tetramer (OVA-tetramer) was obtained from Guangzhou Haozi Biotechnology Co., Ltd. (Guangzhou, China). Chlorpromazine, wortmannin, filipin, and cytochalasin D were purchased from Enzo Biochem, Inc. (New York, USA). Dulbecco's modified Eagle's minimal essential medium (DMEM) and Roswell Park Memorial Institute (RPMI)-1640 medium and mRNA markers were purchased from Thermo Fisher Scientific Inc. (MA, USA). Fetal bovine serum (FBS), phosphate buffer (PBS), and 2-mercaptoethanol were obtained from Gibco (Carlsbad, CA). Other reagents were of analytic grade. E. G7 cells and DC 2.4 and TC-1 cells were purchased from American Type Culture Collection (ATCC). TC-1-GLUC-LMP2 cells were obtained from Mr. Wang Zhan from the Institute of Virology, Chinese Center for Disease Control and Prevention.

2.2 Cell line

DC2.4, TC-1-GLUC-LMP2, and TC-1 cells were cultured in RPMI-1640 medium containing 10% FBS, 1% penicillin, and 1% streptomycin. E. G7 cells were cultured in DMEM containing 10% FBS, 1% penicillin, and 1% streptomycin. All cells were maintained at 37 °C with 5% CO_2 in a cell incubator.

2.3 Experimental animals

C57BL/6 male mice (7–8 weeks old) were purchased from Beijing Huafukang Biotechnology Co., Ltd. The mice were raised in specific pathogen-free (SPF) grade animal rooms and had free access to water and food. All animal experiments were executed according to the protocols approved by the Animal Ethics Committee of Sichuan University.

2.4 Synthesis of mLMP2

The reference amino sequence alignment of LMP2 was obtained from the National Center for Biotechnology Information (NCBI) databases. pST1-LMP2 was linearized with Mfe I. Then, mLMP2 was synthesized using an *in vitro* transcription method by transcription from linearized DNA templates. The concentration of mRNA was determined by absorbance at 260 nm.

2.5 Preparation of LPX

The blank liposomes (LPs) were prepared by a thin-film dispersion method. Briefly, the lipid materials and Chol were dissolved in 2 mL dichloromethane at a molar ratio of 1:1. Then, the clear solution was subjected to a rotary evaporator (R-200, Buchi). After the organic solution was removed, the thin film was hydrated with 2 mL hydration medium at 60 °C for 40 min. Subsequently, the coarse lipid suspension was homogenized using a probe ultrasonic instrument (VCX130, Sonics) at 100 W for 3 min. Uniform LPs were obtained by filtering through a 0.22 μm syringe filter. Finally, the mRNA was encapsulated into LPs by incubation at an N/P ratio of 3:1 to obtain the LPX.

2.6 Characterization of LPs and LPX

The average particle sizes and zeta potentials of LPs were measured using a Malvern Laser Particle Size Analyzer (Zetasizer Nano ZS 90, Malvern, UK). All samples were measured for 3 runs at a fixed angle of 90° at 25 °C.

The morphology was observed using transmission electron microscopy (TEM) (Tecnai-F20, FEI, Netherlands). One drop of the diluted sample was dropped on a 300-mesh grid. Then, the

sample was stained with 1% (*w/v*) phosphotungstic acid before observation.

2.7 Gel electrophoresis

Agarose (0.4 g) was added to 36 mL 1× TAE buffer. The mixture was heated in a microwave oven for 2 min. After cooling to approximately 60 °C, the solution was poured into a gel plate with a gel thickness of 0.5 cm, and a comb was inserted to form gel holes. After the agarose gel was denatured, 10 μL of the samples was added to the gel holes and separated by electrophoresis. When the electrophoresis was stopped, the gel was removed and observed in a gel imaging analyzer (Gel Doc2000, Bio-Rad).

2.8 Storage stability

Storage stability was performed by storing LPX-mLMP2 at 4 °C. On days 0, 7, 14, and 21, the particle size and zeta potential of the samples were detected as described in Section 2.6. The samples were also observed using gel electrophoresis to test mRNA leakage. In addition, the transfection efficiency of LPX after storage for different days was evaluated using fluorescence microscopy and flow cytometry (NovoCyteTM, ACEA Biosciences, Inc.) as described in Section 2.11.

2.9 Effect of serum on LPX-mLMP2

First, LPX-mLMP2 was mixed with 20% serum at a volume ratio of 1:1. After incubation at 37 °C for 2 h, the samples were centrifuged at 4 °C for 60 min with a rotation speed of 10,000 rpm. Then, the supernatants were removed, and the residues were resuspended in saline. LPX-mLMP2 dispersed in saline was used as a control. Subsequently, the particle size and zeta potential were determined as described in Section 2.6.

LPX-mLMP2 stability in serum was investigated by mixing LPX-mLMP2 with serum at a volume ratio of 1:1 and incubating at 37 °C. At 2, 5, 10, and 30 min, and 1 and 2 h, the samples were withdrawn and analyzed using gel electrophoresis as described in Section 2.7.

2.10 Cellular uptake

A cellular uptake study was performed using mCy5, a commercially available Cy5-conjugated mRNA. LPX-mCy5 was prepared as described in Section 2.5. DC 2.4 cells were seeded in 24-well plates at a density of 1×10^5 cells/well. After culturing for 24 h, the cells were incubated with LPX-mCy5 (with 1 μg mCy5 for each well). At different time intervals (0.5, 1, 2, 4, and 6 h), the cells were collected and washed with cold PBS three times. Thereafter, the samples were subjected to flow cytometry.

Moreover, the endocytosis pathways of LPX-mCy5 were studied using different inhibitors, including filipin (1.25 μg/mL, blocking caveolae-mediated endocytosis), cytochalasin-D (2.5 μg/mL, blocking actin-associated macropinocytosis), wortmannin (2 μg/mL, blocking phosphatidylinositol 3-kinase-associated macropinocytosis), and chlorogromazine (5.0 μg/mL, blocking clathrin-mediated endocytosis). The cells were first incubated with the inhibitors at 37 °C for 0.5 h. Then, the inhibitors were replaced with LPX-mCy5 and maintained for another 2 h. Finally, the cells were collected and analyzed using flow cytometry.

2.11 mRNA transfection efficiency study

The transfection efficiency of LPX was investigated using mGFP as a model. DC 2.4 is a commercial murine bone marrow-derived dendritic cell that can be stably passaged and is commonly used in transfection experiments. Briefly, DC 2.4 cells were seeded in 6-well plates at a density of 2×10^5 cells/well. After incubation for 24 h, the cells were transfected with LPX-mGFP. The amount of mRNA was 1 μg for each well. 24 h later, the GFP signal in the cells was observed under a fluorescence microscope. Then, the cells were collected and analyzed using flow cytometry. The transfection efficiency was obtained directly from the flow cytometry pattern.

2.12 Antigen expression

Antigen expression is an important procedure for mRNA vaccines. In this experiment, TC-1 cells were used to verify the antigen expression of LPX-mLMP2. TC-1 cells were seeded in 6-well plates at a density of 2×10^5 cells/well. 24 h later, LPX-mLMP2 was added to the well, with an mRNA amount of 1 μg for each well. After incubation for 24 h, the cells were collected and washed twice with PBS. Since LMP2 is a membrane protein, the samples were incubated with 1 μL of PE-EBV-LMP2 antibody directly without fixation and improving the permeability of the cell membrane. The samples were then subjected to flow cytometry.

2.13 Antigen presentation

The *in vitro* antigen presentation study was conducted using bone marrow-derived dendritic cells (BMDCs), which were usually used for antigen presentation studies. BMDCs collected from the tibia and femur of C57BL/6 mice were treated with a precooled erythrocyte lytic solution for 10 min. Then, the cells were cultured in 10 mL medium containing 10% FBS, 1% penicillin/streptomycin, 1% 2-mercaptoethanol, 89% RPMI-1640 medium, and 0.02 μg GM-CSF. After culturing for 8 days, cells with high purity and a low activation rate were used for the antigen presentation study. In this experiment, mOVA was used because it lacks commercial detection agents for peptide-MHC (pMHC) of LMP2 epitopes. BMDCs were seeded into 24-well plates at a density of 4×10^6 cells/well. After incubation at 37 °C for 2 h, LPX-mOVA was added to the wells. 24 h later, the cells were collected, washed with PBS, and labeled with anti-mouse CD16/32 antibody, PE-anti-mouse CD11c antibody, and APC-anti-mouse SIINFEKL/H-2Kb 25-D1.16 antibody. After washing with PBS, the samples were analyzed using flow cytometry.

The *in vivo* antigen presentation study was performed by collecting the spleen of the immunized mice and making splenocyte suspensions. Then, the cells were handled as described above.

2.14 *In vivo* biodistribution and LPX expression

LPs encapsulated with DiD (LPs-DiD) were prepared via a thin-film dispersion method as described in Section 2.5. Then, LPs-DiD was mixed with mLMP2 to obtain LPX-DiD. Subsequently, LPX-DiD was diluted with saline and injected intravenously into the mice. After 6 h, the mice were sacrificed, and tissues such as the heart, liver, spleen, lung, kidney, and lymph nodes were isolated. The tissues were observed using an IVIS Spectrum living image system (PerkinElmer Co. Ltd., America).

In vivo expression of LPX was conducted using mLUC. First, mLUC was encapsulated in LPs to prepare LPX encapsulated with mLUC (LPX-mLUC). Then, LPX-mLUC was injected intravenously into the mice. 6 h later, D-luciferin was injected intraperitoneally. After another 10 min, the mice were sacrificed, and the tissues were isolated and observed using an IVIS spectrum living image system.

2.15 Pharmacodynamic study

TC-1-GLUC-LMP2 cells expressing the LMP2 antigen were used to establish a tumor-bearing mouse model. Specifically, C57BL/6 mice were randomly divided into four groups. Each mouse was injected with a suspension of 1×10^7 TC-1-GLUC-LMP2 cells in

PBS into the right flank. Mice with subcutaneous tumors ranging from 250 to 300 mm^3 were subjected to treatment. For cancer therapy, intravenous injection is a common delivery route with good immunization [14]. As reported, TCR and interferon (IFN) signaling activation were dependent on the route of mRNA administration, which ultimately impacted CTL activation. It was suggested that mRNA vaccination via intravenous injection could avoid the adverse effects of innate immunity inherent in mRNA and promote $CD8^+$ T-cell responses [19, 33]. Thus, we immunized the mice by intravenous injection. An irrelevant mRNA (mIR) was used as a negative control. The mice were immunized three times at 5-day intervals with saline, mLMP2, LPX-mIR, or LPX-mLMP2 at an mRNA dose of 30 μg/mouse (all the formulations were diluted with saline before injection). Body weight and tumor volume were monitored since the first vaccination. The tumor volume was calculated according to Eq. (1)

$$V = w^2 \times l/2 \quad (1)$$

where w and l are the width and length of the tumor as measured by a caliper.

Five days after the third vaccination, the mice were sacrificed. Tissues such as the heart, liver, spleen, lung, and kidney were isolated and weighed. The organ index of each tissue was calculated according to Eq. (2)

$$\text{Organ index} = \text{organ weight}/\text{body weight} \quad (2)$$

Subsequently, the spleen and lymph nodes were collected to determine the maturity of DCs and the amount of CTLs, respectively. Moreover, the organs were cut into slices and stained with hematoxylin and eosin (H&E) for pathological study. The blood of each mouse was collected by eyeballs, and several biochemical indexes, such as alanine aminotransferase (ALT), aspartic acid aminotransferase (AST), total protein (TP), uric acid (UA), and urinary anhydride (UREAL) were assayed.

2.16 E. G7 tumor-bearing mice establishment and antigen-specific T-cell determination

E. G7 tumor-bearing mice were established by injecting E. G7 cells subcutaneously into the right flank with a cell suspension of 1×10^6 cells in PBS. Mice with tumors of approximately 200 mm^2 were subjected to treatment. In this experiment, LPX-mOVA was used as the therapeutic vaccine. The vaccination regimen was similar to that described in Section 2.14. Eight days after the third vaccination, the mice were sacrificed. The spleen, lymph node, and tumor were collected and detected for antigen presentation and antigen-specific T cells.

Briefly, single spleen, lymph node, and tumor cells were collected and treated with erythrocyte lysate solution for 10 min. Then, the cells were washed twice with PBS. The cells were subsequently labeled with 1 μL FITC-anti-mouse CD3, 1 μL APC-anti-mouse CD8a, and 1 μL H-2kB OVA tetramer SIINFKL/H-2Kb, and kept in the dark at 4 °C for 40 min. Thereafter, the samples were washed with PBS twice and detected using flow cytometry.

2.17 Statistical analysis

The statistical significance of the results was calculated using a two-tailed Student's t test. A p value less than 0.05 was considered statistically significant.

3 Results and discussion

3.1 Preparation and characterization of LPX

EBNA1, LMP1, and LMP2 are the antigen proteins consistently expressed in NPC [25]. EBNA1 maintains EBV DNA in infected cells; however, it also contains a large glycine/alanine repeat domain that could reduce the recognition of $CD4^+$ and $CD8^+$ T cells and result in tumor immune escape [27, 34]. LMP1 is present only in a portion of NPC biopsies, with lower expression in tumor cells [35]. LMP2 is expressed in over 98% of NPC biopsies. It also contains many $CD8^+$ T-cell epitopes and limited $CD4^+$ T-cell epitopes and is considered a promising therapeutic target. Thus, in this study, we developed a synthetic mRNA expressing full-length LMP2, with the optimal codons and a secretion signal sequence to promote immunogenicity and antigen presentation for NPC immunotherapy.

LPs were then prepared using a thin-film dispersion method [36]. Meanwhile, LPX was obtained by mixing LPs and mRNA physically with an N/P ratio of 3. In the preparation process, the hydration medium seemed to be a significant component for the formation of LPs and LPXs. Thus, four kinds of media, H_2O (LP-H_2O), saline (LP-saline), 5% glucose (LP-Glu), and PBS (LP-PBS), were investigated. DOTAP was used as the lipid, and the commercial cationic carrier Lipofectamine 2000 (Lipo) was used as a control. As shown in Fig. 1(a), LP-saline and LP-PBS had larger particle sizes of over 200 nm, while LP-H_2O and LP-Glu exhibited smaller particle sizes of approximately 60 and 100 nm, respectively. The zeta potentials of LP-H_2O and LP-Glu were approximately 34 mV, while LP-saline and LP-PBS had higher zeta potentials. The results indicated that the ions existing in the medium may increase the particle sizes and zeta potentials of LPs. This phenomenon may be due to the adsorption of anions onto the surface of the cationic liposomes and result in a fusion or cross-linking state [37]. The electrophoretogram (Fig. 1(b)) showed that LP-saline and LP-Glu could not efficiently encapsulate the mRNA. This may be because the binding of anions on the head groups of the lipids occupied the binding sites for mRNA [38]. The transfection activities of LPX in DC2.4 cells were also studied. As shown in Fig. 1(c), the transfection efficiencies of LPX-H_2O and LPX-Glu were over 80%, which were similar to that of Lipo. LPX-saline and LPX-PBS had much lower transfection efficiencies of approximately 20%. This may be because LPX-H_2O and LPX-Glu had higher encapsulation rates and smaller particle sizes that facilitated cellular uptake. In addition, although LPX-H_2O and LPX-Glu had similar transfection efficiency, the median fluorescence intensity (MFI) of LPX-H_2O was higher than that of LPX-Glu, which meant that the LPX-H_2O group can translate more GFP per cell. As LPX-H_2O had a smaller particle size and higher transfection activities, H_2O was used as the hydrated medium.

Cationic phospholipid materials are optimum carrier materials for nucleic acid drug delivery [23]. Therefore, the species of cationic lipids were also optimized. As shown in Fig. 1(d), the particle sizes of the LPXs with different cationic lipids were in the order LP-DOTAP < LP- N-[1-(2,3-dioleyloxy)propyl]-N,N,N-trimethylammonium chloride (DOTMA) < LP-DC-Chol < LP-G0-C14. In addition, LP-DOTAP exhibited the highest zeta potential. The electrophoretogram (Fig. 1(e)) showed that, at the ratio of N/P = 3, all the cationic lipids could encapsulate mRNA efficiently without any free mRNA. However, the transfection efficiencies and MFI showed differences (Fig. 1(f)). LPX-G0-C14 showed a slightly higher transfection efficiency but a lower MFI than LPX-DOTMA. We speculated that LPX-G0-C14 was more easily taken up by DC 2.4 than LPX-DOTMA, while LPX-DOTMA was more likely to escape from lysosomes, resulting in a higher MFI. LPX-DOTAP showed the highest transfection efficiency and MFI, while LPX-DC-Chol showed the lowest. This may be due to the smaller particle size and higher surface charge of LP-DOTAP, making it easier for it to interact with the cell membrane and be

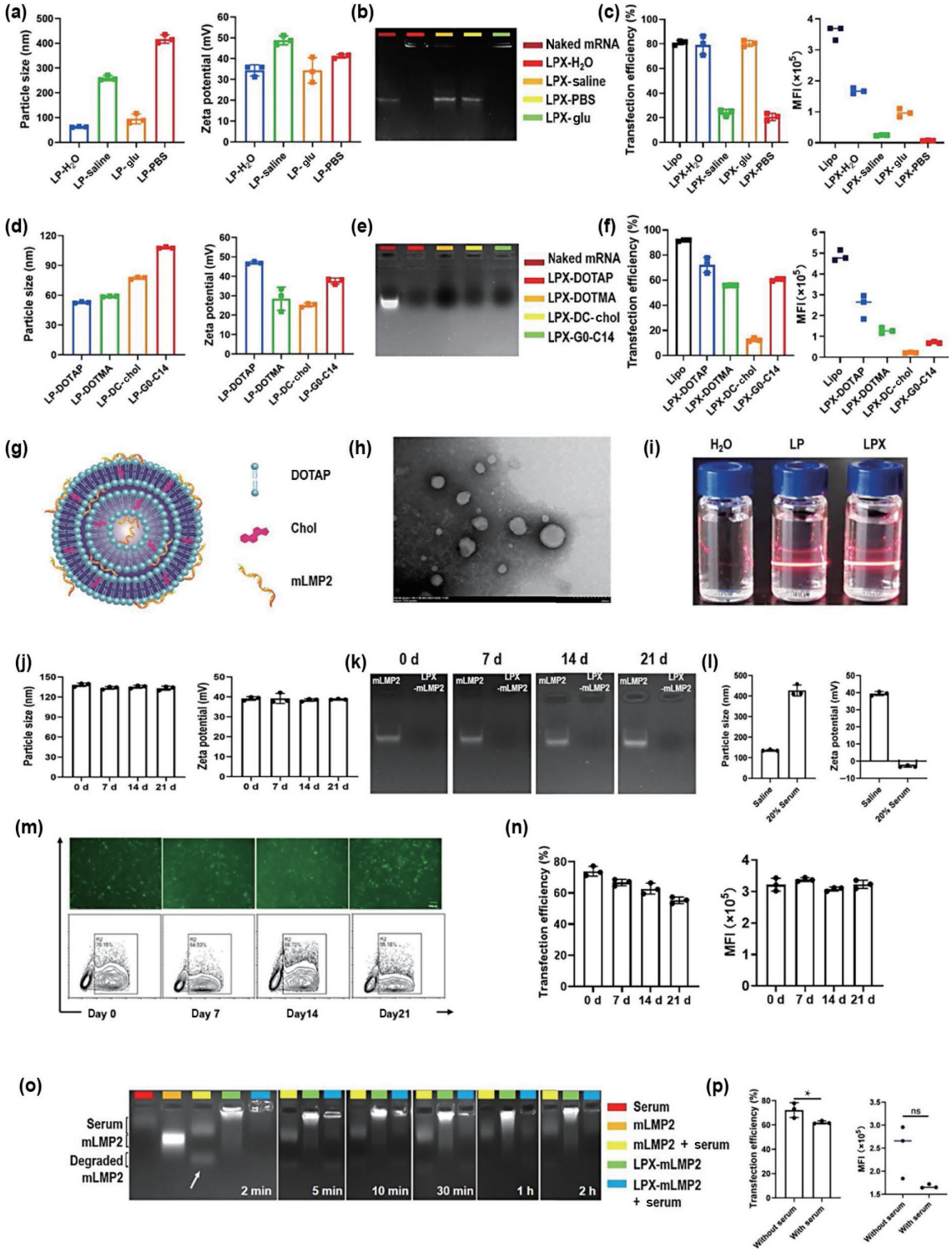

Figure 1 A lipid-based mRNA vaccine (LPX-mLMP2) was developed and characterized. In the preparation process, the hydration medium showed a great influence on the LPX. mGFP was used to optimize the formulation. The particle size and zeta potential (a), electrophoretogram (b), and transfection activities of LPX-mGFP with different hydrated media in DC2.4 cells (c) were investigated. In addition, to optimize the cationic lipids, the particle size and zeta potential (d), electrophoretogram (e), and transfection activities of LPX-mGFP with different kinds of cationic lipids (f) were studied. Based on the schematic image of LPX-mLMP2 (g), the TEM image (h) and Tyndall effect (i) further presented the internal structure and exterior of LPX-mLMP2. The storage stability was investigated by keeping LPX-mLMP2 at 4 °C. The particle sizes, zeta potentials (j), and encapsulation efficiencies (k) were determined on days 0, 7, 14, and 21. The influence of serum protein on LPX-mLMP2 was studied. The particle size and zeta potential of LPX-mLMP2 dispersed in saline and 20% serum were determined (l). Then, fluorescence microscopy (m) and flow cytometry analysis (m) were performed to investigate the mRNA transfection stability in DC2.4 cells. LPX-mLMP2 was mixed with serum at a volume ratio of 1:1, and mRNA degradation was monitored at different time intervals (o). The transfection activities of LPX-mGFP in the medium with/without serum were determined in DC2.4 cells (*$p < 0.05$) (p).

internalized into the cells. Therefore, DOTAP was used as the optimal cationic lipid.

LPX-mLMP2 was then prepared using DOTAP with H_2O as the dispersion medium. The particle size and PDI were 133.57 ± 2.10 nm and 0.188 ± 0.005, respectively. The zeta potential of LPX-mLMP2 was 39.20 ± 2.52 mV. The TEM morphology (Fig. 1(h)) showed that LPX-mLMP2 exhibited a multilayer capsule structure. In addition, the preparations showed the Tyndall effect

under a red laser (Fig. 1(i)), revealing that LPX-mLMP2 existed as a colloidal system.

3.2 Storage and serum stability of LPX

The storage stability of LPX-mLMP2 was studied by maintaining the formulations at 4 °C. From the results (Fig. 1(j)), the particle sizes and zeta potentials of LPX-mLMP2 were unchanged. mLMP2 was encapsulated in LPX-mLMP2 with little leakage for 21 days (Fig. 1(k)). In addition, the transfection of LPX was studied using LPX-mGFP. After 21 days, large amounts of GFP were expressed (Fig. 1(m)). Furthermore, there was no significant decrease in transfection efficiency with time, and the MFIs were almost unchanged (Fig. 1(n)). These results indicated that LPX-mLMP2 could be physically stable for at least 21 days.

Moreover, the serum protein carries negative charges, making it adsorbed on the surface of LPX through electrostatic interactions. Thus, the effect of serum on LPX was also investigated. As shown in Fig. 1(l), after incubation with 20% serum, the particle size of LPX-mLMP2 increased from 136.10 ± 3.03 to 426.93 ± 26.58 nm, while the zeta potential decreased from 39.40 ± 1.15 to −2.99 ± 0.55 mV.

The stability of LPX-mLMP2 in serum is shown in Fig. 1(o). In the electrophoretograms, the serum presented as a dispersive band, and free mLMP2 exhibited a single band. When mLMP2 was incubated in serum, a degradation band was observed after 2 min. Then, the degradation band disappeared after 5 min, which may indicate that mLMP2 was fully degraded. LPX-mLMP2 showed a bright band on the well. After incubation with serum for 2 min, there was barely any degradation band, suggesting that LPX improved the serum stability of mRNA. When incubated for 5 min, most of the LPX-mLMP2 remained in the well, while a small amount of mLMP2 was released and degraded. Moreover, the bands of LPX-mLMP2 in the well became shallower over time, and the degradation band almost disappeared. After incubation for 1 h, LPX-mLMP2 was degraded.

The transfection activity study of LPX in the medium with/without serum was performed in DC 2.4. As shown in Fig. 1(p), in the medium with serum, the transfection activity was reduced from 70% to 60%. This may be due to the degradation of mRNA under serum conditions, as well as the adsorption of serum proteins onto the surface, reducing cellular uptake. Even so, over 60% of cells were transfected, suggesting that LPs could provide a protective effect of mRNA *in vivo*.

3.3 Cellular uptake of LPX

The cellular uptake of LPX was studied using mCy5. As shown in Fig. 2(b), the uptake amount of LPX-mCy5 increased over time and reached the maximum amount at 4 h. The mechanistic study (Fig. 2(c)) showed that filipin and chloropromazine could significantly ($p < 0.05$ and $p < 0.001$) inhibit the uptake of LPX-

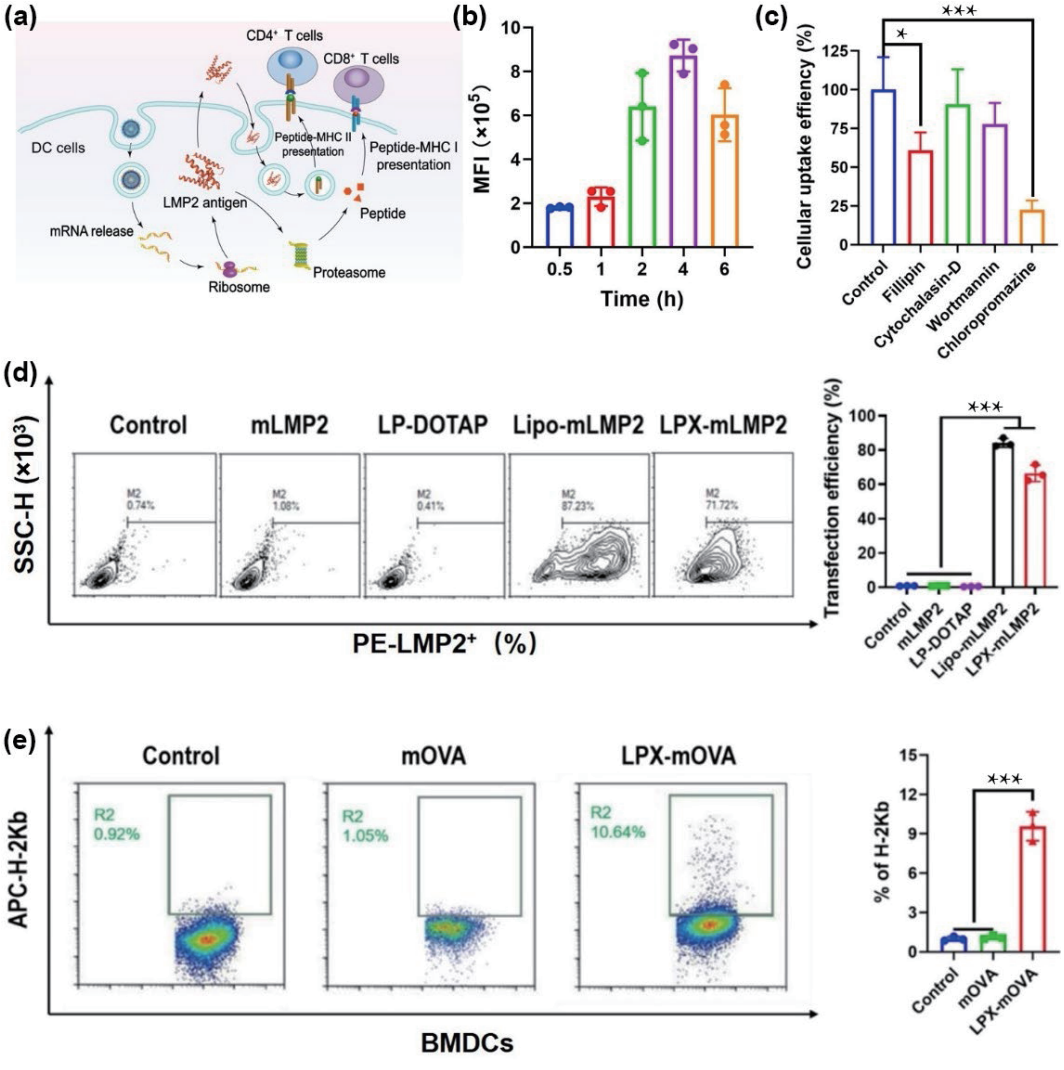

Figure 2 Cellular uptake behavior, antigen expression, and presentation of LPX. Schematic graph of LPX behavior in DCs (a). Cellular uptake of LPX-mCy5 in DC2.4 cells after incubation for 0.5, 1, 2, and 4 h ($n = 3$) (b). Cellular uptake mechanism study in DC2.4 cells after incubation with various inhibitors ($n = 3$) (c). Antigen expression of LPX-mLMP2 in TC-1 cells ($n = 3$) (d). Antigen presentation of LPX-mOVA in BMDCs ($n = 3$, $^*p < 0.05$, $^{***}p < 0.001$) (e).

mCy5, which meant that caveolin- and clathrin-mediated pathways were involved in the cellular uptake of LPX-mCy5.

3.4 Antigen expression and presentation

The antigen expression of mLMP2 is shown in Fig. 2(d). Untreated TC-1 cells were used as a control. The transfection efficiencies of mLMP2 and blank LPs were similar to that of the control. This was because mLMP2 was easily degraded and hardly internalized into cells. Lipo-mLMP2 and LPX-mLMP2 had transfection efficiencies of 84.3% and 66.5%, respectively, which were higher than that of naked mLMP2. This suggested that the cationic carriers could facilitate the expression of mLMP2. However, although lipo showed better transfection efficiency than LPs, it has large toxicity that cannot be applied *in vivo*. Antigen expression was the crucial step of immunization because only when the antigen was successfully expressed would it activate the immunoreaction of the body. However, naked mRNA is vulnerable to degradation in the presence of nucleases. Cationic lipids such as DOTAP are efficient anchors to load mRNA into a lamellar lipid matrix and improve protein expression.

Once the antigen is expressed in DCs, it is processed into various immunogenic peptides. The peptides were then complexed with the MHC molecules and presented to the surface of the DCs for immune stimulation. In this study, an antigen presentation study was performed using BMDCs. BMDCs were differentiated with GM-CSF as described previously [39]. Before the experiment, the BMDCs were cultured for 8 days. On the last day, clumps of cell colonies could be observed under the microscope, which indicated that the addition of GM-CSF promoted the differentiation and the production of BMDCs (Fig. S1 in the Electronic Supplementary Material (ESM)). The purity of BMDCs was 81.25%, and the positive rates of $CD80^+$ cells and $CD86^+$ cells were low, indicating that the BMDCs were immature. These BMDCs could be used for the antigen presentation study. As there was no commercial detection reagent available for LMP2 epitopes, mOVA was used as the model mRNA. The OVA CD8 epitope (SIINFEKL) is present in the context of MHC I $H\text{-}2K^b$ on the surface of BMDCs [40]. As shown in Fig. 2(e), the presentation of mOVA encapsulated in LPs was approximately 9%, which was higher than that of naked mOVA. These results suggested that LPX-mLMP2 could express mLMP2 in APCs and be presented on the surface of APCs, which would further be recognized by antigen-specific CTLs.

3.5 Biodistribution and LPX translation *in vivo*

To visualize the biodistribution of LPX, we prepared LPX-mLMP2/DID and injected it intravenously into the mice. After 6 h, the tissues were isolated and observed. As shown in Fig. 3(a), LPX-mLMP2/DiD accumulated in the liver, spleen, and lung. This may be due to the passive targeting properties of the nanoparticles, which were easily phagocytosed by the mononuclear macrophage system. Meanwhile, LPX-mLUC was used to investigate the translation efficiency *in vivo* through bioluminescence imaging. As shown in Fig. 3(b), the expression of mLUC was predominantly in the lung and spleen, and little was shown in the liver. This was similar to another well-established lipid composition DOTMA and 1,2-dioleoyl-sn-glycero-3-phosphoethanolamine (DOPE) [19]. The spleen plays an important role in immune regulation, where the highest density of DCs exists. Thus, the expression of antigen in DCs from the spleen was in favor of stimulating an adaptive immune response *in vivo*.

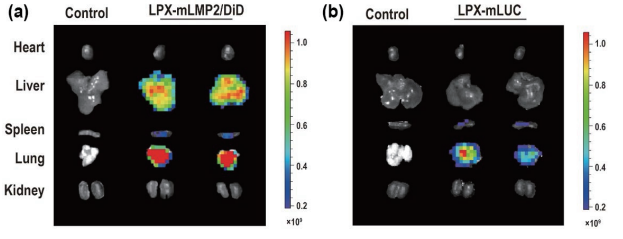

Figure 3 LPX was distributed and expressed in the spleen. Representative fluorescence images of biodistribution (a) and transfection *in vivo* (b) of LPX in C57BL/6 mice after intravenous injection.

3.6 Pharmacodynamic study

The vaccination effect of LPX-mLMP2 was studied in C57BL/6 mice. TC-1-GLUC-LMP2 cells, which highly express LMP2 (Fig. S2 in the ESM), were used for the establishment of NPC tumor-bearing mice. The mice were vaccinated with LPX-mLMP2 three times at five-day intervals through intravenous injection (Fig. 4(a)). The dosage was 30 μg of mLMP2 for each mouse. During the treatment, tumor volumes were monitored every three days. As shown in Figs. 4(b) and 4(c), the tumor volume grew rapidly when treated with saline and free mLMP2, indicating that the free mRNA had almost no antitumor effect. As the tumor volumes for the saline and free mLMP2 groups were too large, although the mice were physically and mentally healthy, they were sacrificed according to ethical guidance. After administration of LPX-mIR, the growth of tumors was inhibited to some extent. This may be due to the immunologic adjuvant effect of cationic liposomes, which would enhance the body's immune response [41]. Surprisingly, LPX-mLMP2 could significantly reduce the growth of tumors and exhibited superior tumor immunotherapy effects. On the fifth day of the last vaccination, the mice were harvested. The spleen of each mouse was isolated and detected for maturation. As shown in Fig. 4(d), the percentage of $CD11c^+$ DCs for LPX-mLMP2 was significantly higher than those of the control group and LPX-mIR group ($p < 0.001$). The MFI of $CD86^+$ DCs was also significantly higher for LPX-mLMP2 ($p < 0.001$). These results indicated that the expression and presentation of LPX-mLMP2 stimulated the maturation of DCs in the spleen. Meanwhile, the numbers of $CD4^+$ T cells and $CD8^+$ T cells from inguinal lymph nodes were also increased (Fig. S3 in the ESM). These results indicated that LPX-mLMP2 could mature DCs *in vivo* and activate the proliferation of $CD4^+$ T cells and $CD8^+$ T cells to kill tumor cells.

Limited to the detection method of LMP2-specific T cells, we used mOVA to investigate the production of antigen-specific T cells. OVA-expressing E. G7 cells were used to establish tumor-bearing mice. The dosage regimen was similar to before (Fig. 5(a)). From the results (Fig. 5(b)), LPX-mOVA significantly ($p < 0.001$) inhibited tumor growth. It seemed that LPX-mOVA had a better antitumor effect than LPX-mLMP2. This might be attributable to different models. After TC-1-GLUC-LMP2 inoculation, tumor growth was very rapid. For humanitarian consideration, mice in the control group and mLMP2 group had to be euthanized 9 days before the end of treatment. For E. G7 tumor-bearing mice, the tumors showed steady growth.

The spleens were harvested to investigate antigen presentation and antigen-specific T cells. As shown in Fig. 5(c), antigen presentation of LPX-mOVA was detected in the spleen tissue ($p < 0.05$), indicating that LPX-mOVA could be expressed successfully and presented the epitope *in vivo*. The numbers of activated OVA-specific T cells in the spleen and tumor, which were pivotal for killing tumor cells, were significantly higher ($p < 0.001$) in the LPX-mOVA than in the control group (Figs. 5(d) and 5(e), and the gating strategy for the analysis of antigen-specific CTLs is shown in Fig. S4 in the ESM). These results proved that LP-DOTAP was a favorable candidate carrier for delivering mRNA for the treatment of cancer.

NPC has a complex TME, where $CD4^+$ T cells and $CD8^+$ T cells

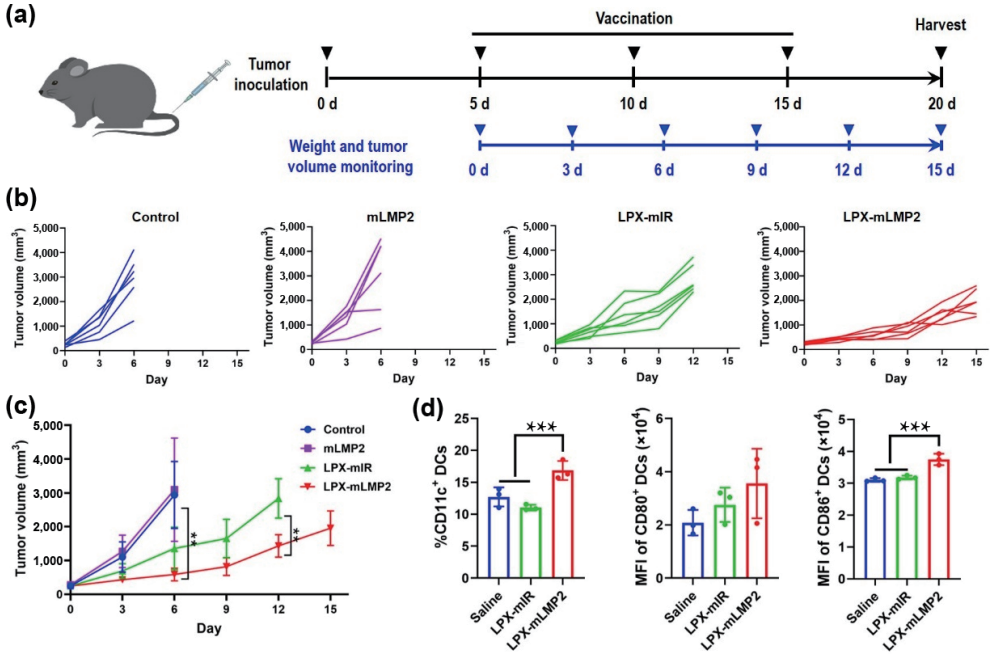

Figure 4 LPX-mLMP2 inhibited tumor growth. Vaccination regimen: TC-1-GLUC-LMP2-tumor-bearing mice were vaccinated three times at five-day intervals. During the vaccination period, the weight and tumor volume were monitored every three days. Then, five days after the last vaccination, the mice were sacrificed (a). Tumor volume of each mouse ($n = 6$) (b) and statistical volumes ($n = 6$) (c) after injection with saline, mLMP2, LPX-mIR, and LPX-mLMP2. The maturation of DCs from the spleen after three vaccinations ($^{**}p < 0.01$, $^{***}p < 0.001$) (d).

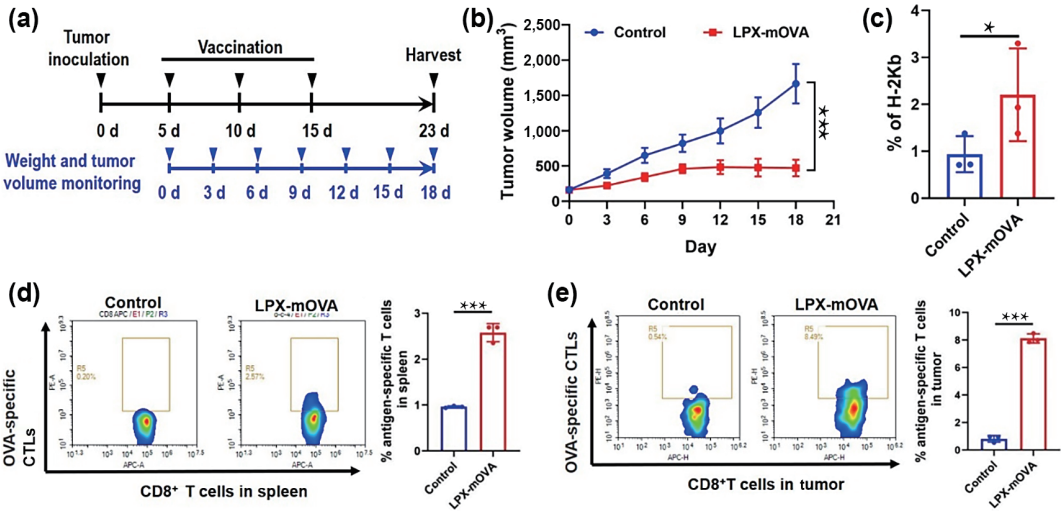

Figure 5 mOVA was used to study the immunologic mechanism. The vaccination regimen is presented in (a). Tumor volumes in E. G7 tumor-bearing mice when vaccinated with LPX-mOVA ($n = 6$) (b). Antigen presentation in DCs from the spleen (c) and antigen-specific T-cell proliferation in the spleen (d) and tumor (e) were determined after the tissues were harvested ($^{*}p < 0.5$, $^{***}p < 0.001$).

together comprise over half of the infiltrating lymphocytes [42]. Other immune cells, including B-lymphocytes, macrophages, and natural killer cells, account for a small proportion. However, the presence of immunosuppressive lymphocytes always results in a failure to induce a strong antitumor immune response [43]. Several strategies have been developed to trigger antitumor immune responses, including immunogenic cell death induced by calcium ion nanomodulators [44] and increased tumor infiltrating lymphocytes (TILs) [45]. In patients with NPC, a higher density of TILs predicted a favorable free survival and overall survival rate [46]. However, due to EBV infection and tumor cells, TILs in NPC are highly activated and exhausted [47]. Thus, increasing the accumulation of antigen-specific TILs in the tumor site is critical for NPC. In our study, OVA-specific TILs were much more increased in tumors. Combining the antitumor effect of LPX-mLMP2 in an LMP2-expressing tumor model, LPX-mLMP2 appeared to be a valuable vaccine strategy for NPC immunotherapy.

In addition, the results also demonstrated the possible immunization process for tumor immunotherapy. After LPX-mLMP2 was injected into mice, it accumulated in the spleen and expressed LMP2 in DCs. On the one hand, DCs could deal with LMP2 and form the pMHC I-LMP2 epitope, which could be recognized by $CD8^+$ T cells. On the other hand, LMP2 may be expelled and reabsorbed by DCs, processed into the pMHC Ⅱ-LMP2 epitope and recognized by $CD4^+$ T cells. Then, $CD4^+$ T cells and $CD8^+$ T cells differentiated and proliferated into LMP2-specific CTLs. LMP2-specific CTLs recognize tumor cells expressing the LMP2 antigen and kill them. These results showed an efficient and accurate immunotherapeutic effect of LPX-mLMP2.

3.7 Safety evaluation

The safety of LPX-mLMP2 was evaluated. The cytotoxicity assay (Fig. 6(a)) showed that it was not cytotoxic to DC 2.4 when the

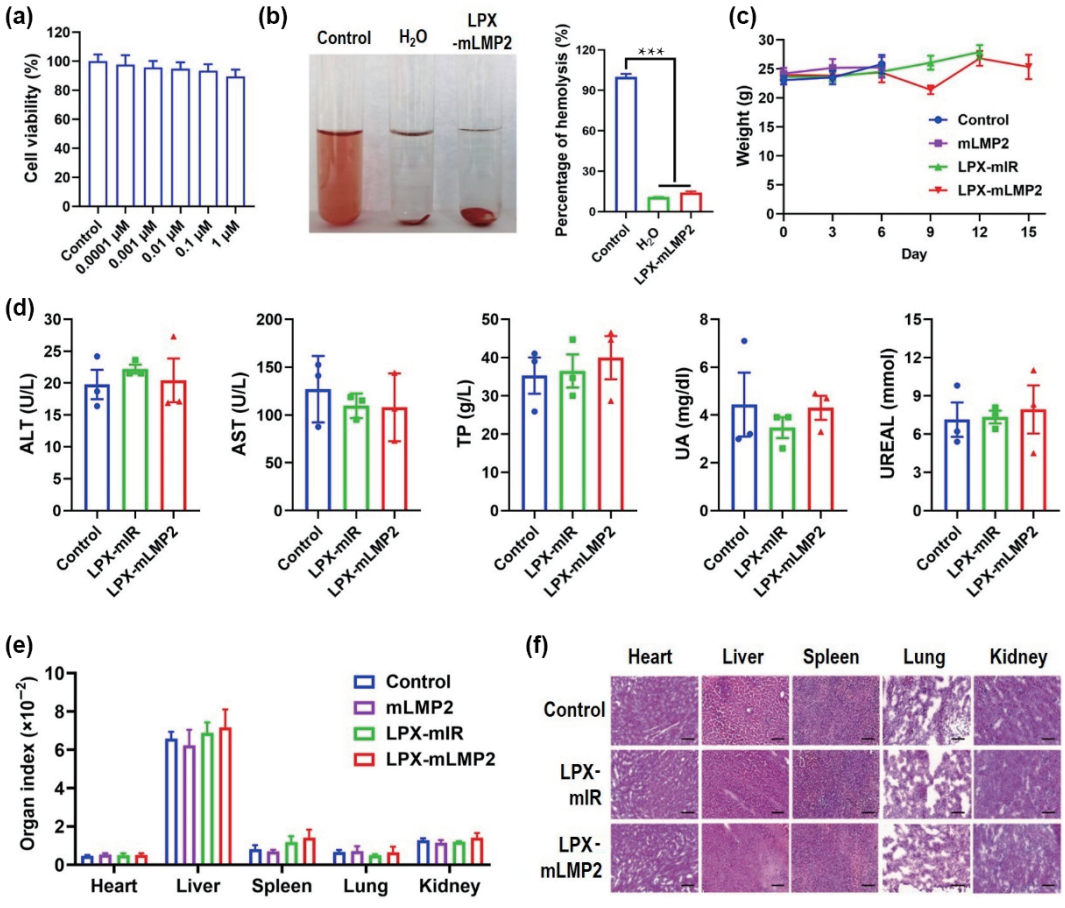

Figure 6 LPX-mLMP2 had barely any cytotoxicity and was safe in mice. Cell viability of DC 2.4 cells after incubation with various concentrations of LPX-mLMP2 (a). Hemolysis analysis of LPX-mLMP2 (b). Body weight monitoring of tumor-bearing mice vaccinated with saline, mLMP2, LPX-mIR, and LPX-mLMP2 (n = 6) (c). Biochemical analysis of ALT, AST, TP, UA, and UREAL in tumor-bearing mice after three vaccinations (d). Organ index (e) and H&E images (f) of isolated tissues, including the heart, liver, spleen, lung, and kidney of tumor-bearing mice after three vaccinations (scale bar = 200 μm) (***$p < 0.001$).

concentration of LPX-mLMP2 was increased to 1 μM. In the hemolysis experiment (Fig. 6(b)), after treatment with pure water, the cells were completely hemolytic, and the solution was red and clear with no erythrocyte precipitation at the bottom of the test tube. However, when treated with saline and LPX-mLMP2, no hemolysis phenomenon was observed, indicating that LPX-mLMP2 had good blood compatibility.

To investigate the safety of LPX-mLMP2 *in vivo*, body weight was monitored during the immunization process. As shown in Fig. 6(c), the body weights were almost unchanged until the mice were harvested. Five days after the third vaccination with LPX-mLMP2, the blood samples were withdrawn. Biochemical assays of ALT, AST, TP, UA, and UREAL were performed. ALT, AST, and TP are always used in liver function tests, while UA and UREAL indicate kidney function. In our study, all the groups showed similar values as the control, suggesting that LPX-LMP2 had little hepatotoxicity and nephrotoxicity.

After vaccination, the tissues were isolated, weighed, and examined via H&E staining. From Fig. 6(e), there were no significant changes in organ indexes, revealing that the organs had not been damaged after vaccination. Moreover, the H&E staining results (Fig. 6(f)) showed that there were no obvious histopathologic differences in the main organs. These data demonstrated that LPX-mLMP2 was safe *in vivo*.

4 Conclusion

This was the first time that we reported mLMP2-encapsulated cationic liposomes for the immunotherapy of NPC. The mRNA vaccine could efficiently express and present LMP2 antigen *in vivo*. After vaccination, boosting antigen-specific T cells can be detected in the tumor site, which are the main force against NPC. We have demonstrated that mRNA vaccination is a promising strategy for the immunotherapy of virus-related cancer.

Acknowledgements

The work was supported by the National Key Research and Development Program of China (No. 2021YFE0206600), Sichuan Province Science and Technology Support Program (Nos. 2021YFSY0008 and 2020YFH0065), the Translational medicine fund of West China Hospital (No. CGZH19002), and 1.3.5 project for disciplines of excellence, West China Hospital, Sichuan University (No. ZYGD18020/ZYJC18006).

Electronic Supplementary Material: Supplementary material (methods of cytotoxicity assay, LMP2 expression, hemolysis test, the results of purity and maturity of BMDCs, LMP2 expression, and evaluation of T cells in lymph nodes and gating strategy for CTLs) is available in the online version of this article at https://doi.org/10.1007/s12274-022-5254-x.

References

[1] Sung, H.; Ferlay, J.; Siegel, R. L.; Laversanne, M.; Soerjomataram, I.; Jemal, A.; Bray, F. Global cancer statistics 2020: GLOBOCAN estimates of incidence and mortality worldwide for 36 cancers in 185 countries. *CA Cancer J. Clin.* **2021**, *71*, 209–249.

[2] Tyagi, R. K.; Parmar, R.; Patel, N. A generic RNA pulsed DC based approach for developing therapeutic intervention against nasopharyngeal carcinoma. *Hum. Vaccin. Immunother.* **2017**, *13*, 854–866.

[3] Coghill, A. E.; Hildesheim, A. Epstein–Barr virus antibodies and the risk of associated malignancies: Review of the literature. *Am. J. Epidemiol.* **2014**, *180*, 687–695.
[4] Zhu, Q. Y.; Kong, X. W.; Sun, C.; Xie, S. H.; Hildesheim, A.; Cao, S. M.; Zeng, M. S. Association between antibody responses to Epstein–Barr virus glycoproteins, neutralization of infectivity, and the risk of nasopharyngeal carcinoma. *mSphere* **2020**, *5*, e00901–20.
[5] Khanna, R.; Moss, D.; Gandhi, M. Technology insight: Applications of emerging immunotherapeutic strategies for Epstein–Barr virus-associated malignancies. *Nat. Clin. Pract. Oncol.* **2005**, *2*, 138–149.
[6] Dasari, V.; Sinha, D.; Neller, M. A.; Smith, C.; Khanna, R. Prophylactic and therapeutic strategies for Epstein–Barr virus-associated diseases: Emerging strategies for clinical development. *Expert Rev. Vaccines* **2019**, *18*, 457–474.
[7] Zeng, Y.; Si, Y. F.; Lan, G. P.; Wang, Z.; Zhou, L.; Tang, M. Z.; Sj, O. B.; Lan, J.; Zhou, X. Y.; Wang, Y. L. et al. LMP2-DC vaccine elicits specific EBV-LMP2 response to effectively improve immunotherapy in patients with nasopharyngeal cancer. Biomed. Environ. *Sci.* **2020**, *33*, 849–856.
[8] Ge, Y. Y.; Zhou, Z. X.; Wang, X. L.; Zhou, Y. B.; Liu, W.; Teng, Z. P.; Zeng, Y. *In vitro* evaluation of the therapeutic effectiveness of EBV-LMP2 recombinant adenovirus vaccine in nasopharyngeal carcinoma. *Biomed. Pharmacother.* **2020**, *121*, 109626.
[9] Taylor, G. S.; Jia, H.; Harrington, K.; Lee, L. W.; Turner, J.; Ladell, K.; Price, D. A.; Tanday, M.; Matthews, J.; Roberts, C. et al. A recombinant modified Vaccinia Ankara vaccine encoding Epstein–Barr virus (EBV) target antigens: A phase I trial in UK patients with EBV-positive cancer. *Clin. Cancer Res.* **2014**, *20*, 5009–5022.
[10] Feng, C.; Li, Y. J.; Ferdows, B. E.; Patel, D. N.; Ouyang, J.; Tang, Z. M.; Kong, N.; Chen, E. G.; Tao, W. Emerging vaccine nanotechnology: From defense against infection to sniping cancer. *Acta Pharm. Sin. B* **2022**, *12*, 2206–2223.
[11] Thompson, M. G.; Burgess, J. L.; Naleway, A. L.; Tyner, H.; Yoon, S. K.; Meece, J.; Olsho, L. E. W.; Caban-Martinez, A. J.; Fowlkes, A. L.; Lutrick, K. et al. Prevention and attenuation of COVID-19 with the BNT162b2 and mRNA-1273 vaccines. *N. Engl. J. Med.* **2021**, *385*, 320–329.
[12] Islam, M. A.; Rice, J.; Reesor, E.; Zope, H.; Tao, W.; Lim, M.; Ding, J. X.; Chen, Y. H.; Aduluso, D.; Zetter, B. R. et al. Adjuvant-pulsed mRNA vaccine nanoparticle for immunoprophylactic and therapeutic tumor suppression in mice. *Biomaterials* **2021**, *266*, 120431.
[13] Kong, N.; Zhang, R. N.; Wu, G. W.; Sui, X. B.; Wang, J. Q.; Kim, N. Y.; Blake, S.; De, D.; Xie, T.; Cao, Y. H. et al. Intravesical delivery of *KDM6A*-mRNA via mucoadhesive nanoparticles inhibits the metastasis of bladder cancer. *Proc. Natl. Acad. Sci. USA* **2022**, *119*, e2112696119.
[14] Xiong, Q. Q.; Lee, G. Y.; Ding, J. X.; Li, W. L.; Shi, J. J. Biomedical applications of mRNA nanomedicine. *Nano Res.* **2018**, *11*, 5281–5309.
[15] Lin, Y. X.; Wang, Y.; Ding, J. X.; Jiang, A. P.; Wang, J.; Yu, M.; Blake, S.; Liu, S. S.; Bieberich, C. J.; Farokhzad, O. C. et al. Reactivation of the tumor suppressor PTEN by mRNA nanoparticles enhances antitumor immunity in preclinical models. *Sci. Transl. Med.* **2021**, *13*, eaba9772.
[16] Pardi, N.; Hogan, M. J.; Porter, F. W.; Weissman, D. mRNA vaccines—A new era in vaccinology. Nat. Rev. *Drug Discov.* **2018**, *17*, 261–279.
[17] Coolen, A. L.; Lacroix, C.; Mercier-Gouy, P.; Delaune, E.; Monge, C.; Exposito, J. Y.; Verrier, B. Poly(lactic acid) nanoparticles and cell-penetrating peptide potentiate mRNA-based vaccine expression in dendritic cells triggering their activation. *Biomaterials* **2019**, *195*, 23–37.
[18] Uchida, S.; Kinoh, H.; Ishii, T.; Matsui, A.; Tockary, T. A.; Takeda, K. M.; Uchida, H.; Osada, K.; Itaka, K.; Kataoka, K. Systemic delivery of messenger RNA for the treatment of pancreatic cancer using polyplex nanomicelles with a cholesterol moiety. *Biomaterials* **2016**, *82*, 221–228.
[19] Kranz, L. M.; Diken, M.; Haas, H.; Kreiter, S.; Loquai, C.; Reuter, K. C.; Meng, M.; Fritz, D.; Vascotto, F.; Hefesha, H. et al. Systemic RNA delivery to dendritic cells exploits antiviral defence for cancer immunotherapy. *Nature* **2016**, *534*, 396–401.
[20] Vik-Mo, E. O.; Nyakas, M.; Mikkelsen, B. V.; Moe, M. C.; Due-Tonnesen, P.; Suso, E. M. I.; Sæbøe-Larssen, S.; Sandberg, C.; Brinchmann, J. E.; Helseth, E. et al. Therapeutic vaccination against autologous cancer stem cells with mRNA-transfected dendritic cells in patients with glioblastoma. *Cancer Immunol. Immunother.* **2013**, *62*, 1499–1509.
[21] Kubler, H.; Scheel, B.; Gnad-Vogt, U.; Miller, K.; Schultze-Seemann, W.; Vom Dorp, F.; Parmiani, G.; Hampel, C.; Wedel, S.; Trojan, L. et al. Self-adjuvanted mRNA vaccination in advanced prostate cancer patients: A first-in-man phase I/IIa study. *J. Immunother. Cancer* **2015**, *3*, 26.
[22] Li, Z. M.; Xu, W. G.; Yang, J. Z.; Wang, J.; Wang, J. L.; Zhu, G.; Li, D.; Ding, J. X.; Sun, T. M. A tumor microenvironments-adapted polypeptide hydrogel/nanogel composite boosts antitumor molecularly targeted inhibition and immunoactivation. *Adv. Mater.* **2022**, *34*, 2200449.
[23] Feng, X. R.; Xu, W. G.; Li, Z. M.; Song, W. T.; Ding, J. X.; Chen, X. S. Immunomodulatory nanosystems. *Adv. Sci.* **2019**, *6*, 1900101.
[24] Fogg, M. H.; Wirth, L. J.; Posner, M.; Wang, F. Decreased EBNA-1-specific $CD8^+$ T cells in patients with Epstein–Barr virus-associated nasopharyngeal carcinoma. *Proc. Natl. Acad. Sci. USA* **2009**, *106*, 3318–3323.
[25] Dawson, C. W.; Port, R. J.; Young, L. S. The role of the EBV-encoded latent membrane proteins LMP1 and LMP2 in the pathogenesis of nasopharyngeal carcinoma (NPC). *Semin. Cancer Biol.* **2012**, *22*, 144–153.
[26] Zhu, S. L.; Chen, J.; Xiong, Y. R.; Kamara, S.; Gu, M. P.; Tang, W. L.; Chen, S.; Dong, H. Y.; Xue, X. Y.; Zheng, Z. M. et al. Novel EBV LMP-2-affibody and affitoxin in molecular imaging and targeted therapy of nasopharyngeal carcinoma. *PLoS Pathog.* **2020**, *16*, e1008223.
[27] Taylor, G. S.; Steven, N. M. Therapeutic vaccination strategies to treat nasopharyngeal carcinoma. *Chin. Clin. Oncol.* **2016**, *5*, 23.
[28] Meij, P.; Leen, A.; Rickinson, A. B.; Verkoeijen, S.; Vervoort, M. B. H. J.; Bloemena, E.; Middeldorp, J. M. Identification and prevalence of $CD8^+$ T-cell responses directed against Epstein–Barr virus-encoded latent membrane protein 1 and latent membrane protein 2. *Int. J. Cancer* **2002**, *99*, 93–99.
[29] Lei, L.; Li, J. H.; Liu, M. Q.; Hu, X. M.; Zhou, Y.; Yang, S. M. CD40L-adjuvanted DNA vaccine carrying EBV-LMP2 antigen enhances anti-tumor effect in NPC transplantation tumor animal. Cent. Eur. *J. Immunol.* **2018**, *43*, 117–122.
[30] Si, Y. F.; Deng, Z. X.; Lan, G. P.; Du, H. J.; Wang, Y. L.; Si, J. Y.; Wei, J. Z.; Weng, J. J.; Qin, Y. D.; Huang, B. et al. The safety and immunological effects of rAd5-EBV-LMP2 vaccine in nasopharyngeal carcinoma patients: A phase I clinical trial and two-year follow-up. *Chem. Pharm. Bull.* **2016**, *64*, 1118–1123.
[31] Lao, T. D.; Le, T. A. H. Association between *LMP-1, LMP-2*, and miR-155 expression as potential biomarker in nasopharyngeal carcinoma patients: A case/control study in Vietnam. *Genet. Test. Mol. Biomarkers* **2019**, *23*, 815–822.
[32] Xu, X. Y.; Xie, K.; Zhang, X. Q.; Pridgen, E. M.; Park, G. Y.; Cui, D. S.; Shi, J. J.; Wu, J.; Kantoff, P. W.; Lippard, S. J. et al. Enhancing tumor cell response to chemotherapy through nanoparticle-mediated codelivery of siRNA and cisplatin prodrug. *Proc. Natl. Acad. Sci. USA* **2013**, *110*, 18638–18643.
[33] Pollard, C.; Rejman, J.; De Haes, W.; Verrier, B.; Van Gulck, E.; Naessens, T.; De Smedt, S.; Bogaert, P.; Grooten, J.; Vanham, G. et al. Type I IFN counteracts the induction of antigen-specific immune responses by lipid-based delivery of mRNA vaccines. *Mol. Ther.* **2013**, *21*, 251–259.
[34] Frappier, L. Role of EBNA1 in NPC tumourigenesis. *Semin. Cancer Biol.* **2012**, *22*, 154–161.
[35] Brooks, L.; Yao, Q. Y.; Rickinson, A. B.; Young, L. S. Epstein–Barr virus latent gene transcription in nasopharyngeal carcinoma cells: Coexpression of EBNA1, LMP1, and LMP2 transcripts. *J. Virol.* **1992**, *66*, 2689–2697.
[36] Wang, F. Z.; Xiao, W.; Elbahnasawy, M. A.; Bao, X. T.; Zheng, Q.;

Gong, L. H.; Zhou, Y.; Yang, S. P.; Fang, A. P.; Farag, M. M. S. et al. Optimization of the linker length of mannose-cholesterol conjugates for enhanced mRNA delivery to dendritic cells by liposomes. *Front. Pharmacol.* **2018**, *9*, 980.

[37] Siepi, E.; Lutz, S.; Meyer, S.; Panzner, S. An ion switch regulates fusion of charged membranes. *Biophys. J.* **2011**, *100*, 2412–2421.

[38] Ruso, J. M.; Besada, L.; Martínez-Landeira, P.; Seoane, L.; Prieto, G.; Sarmiento, F. Interactions between liposomes and cations in aqueous solution. *J. Liposome Res.* **2003**, *13*, 131–145.

[39] Latchumanan, V. K.; Singh, B.; Sharma, P.; Natarajan, K. *Mycobacterium tuberculosis* antigens induce the differentiation of dendritic cells from bone marrow. *J. Immunol*. **2002**, *169*, 6856–6864.

[40] Lou, B.; De Koker, S.; Lau, C. Y. J.; Hennink, W. E.; Mastrobattista, E. mRNA polyplexes with post-conjugated GALA peptides efficiently target, transfect, and activate antigen presenting cells. *Bioconjugate Chem*. **2019**, *30*, 461–475.

[41] Wang, Y.; Zhang, Z. Q.; Luo, J. W.; Han, X. J.; Wei, Y. Q.; Wei, X. W. mRNA vaccine: A potential therapeutic strategy. *Mol. Cancer* **2021**, *20*, 33.

[42] Huang, S. C. M.; Tsao, S. W.; Tsang, C. M. Interplay of viral infection, host cell factors and tumor microenvironment in the pathogenesis of nasopharyngeal carcinoma. *Cancers* **2018**, *10*, 106.

[43] Feng, X. R.; Xu, W. G.; Liu, J. H.; Li, D.; Li, G.; Ding, J. X.; Chen, X. S. Polypeptide nanoformulation-induced immunogenic cell death and remission of immunosuppression for enhanced chemoimmunotherapy. *Sci. Bull.* **2021**, *66*, 362–373.

[44] Zheng, P.; Ding, B. B.; Jiang, Z. Y.; Xu, W. G.; Li, G.; Ding, J. X.; Chen, X. S. Ultrasound-augmented mitochondrial calcium ion overload by calcium nanomodulator to induce immunogenic cell death. *Nano Lett.* **2021**, *21*, 2088–2093.

[45] Zhao, Y. S.; Deng, J.; Rao, S. F.; Guo, S. P.; Shen, J.; Du, F. K.; Wu, X.; Chen, Y.; Li, M. X.; Chen, M. J. et al. Tumor infiltrating lymphocyte (TIL) therapy for solid tumor treatment: Progressions and challenges. *Cancers* **2022**, *14*, 4160.

[46] Ono, T.; Azuma, K.; Kawahara, A.; Sasada, T.; Matsuo, N.; Kakuma, T.; Kamimura, H.; Maeda, R.; Hattori, C.; On, K. et al. Prognostic stratification of patients with nasopharyngeal carcinoma based on tumor immune microenvironment. *Head Neck* **2018**, *40*, 2007–2019.

[47] Jin, S. Z.; Li, R. Y.; Chen, M. Y.; Yu, C.; Tang, L. Q.; Liu, Y. M.; Li, J. P.; Liu, Y. N.; Luo, Y. L.; Zhao, Y. F. et al. Single-cell transcriptomic analysis defines the interplay between tumor cells, viral infection, and the microenvironment in nasopharyngeal carcinoma. *Cell Res.* **2020**, *30*, 950–965.